Lanthanide Oleates: Chelation, Self-assembly, and Exemplification of Ordered Nanostructured Colloidal Contrast Agents for Medical Imaging

ARTICLE *in* THE JOURNAL OF PHYSICAL CHEMISTRY B · NOVEMBER 2009

Impact Factor: 3.3 · DOI: 10.1021/jp906344u · Source: PubMed

3 AUTHORS:

Guozhen Liu
Central China Normal University
46 PUBLICATIONS **1,079** CITATIONS
SEE PROFILE

Charlotte E Conn
The Commonwealth Scientific and Industri…
41 PUBLICATIONS **738** CITATIONS
SEE PROFILE

Calum J. Drummond
RMIT University
190 PUBLICATIONS **6,992** CITATIONS
SEE PROFILE

Lanthanide Oleates: Chelation, Self-assembly, and Exemplification of Ordered Nanostructured Colloidal Contrast Agents for Medical Imaging

Guozhen Liu,[†] Charlotte E. Conn,[†] and Calum J. Drummond*[,†,‡]

CSIRO Molecular and Health Technologies (CMHT), Private Bag 10, Clayton South MDC, VIC 3169, Australia, and CSIRO Materials Science and Engineering (CMSE), Private Bag 33, Clayton South MDC, VIC 3169, Australia

Received: July 5, 2009; Revised Manuscript Received: September 23, 2009

Eight lanthanide(III) oleates have been prepared and characterized. The chelation and self-assembly structures of these rare-earth oleates have been studied by elemental analysis, Fourier transfer infrared spectroscopy (FTIR), and X-ray powder diffraction (XRD) analysis. Elemental analysis and FTIR results indicate that three oleate anions are complexed with one lanthanide cation and, with the exception of anhydrous cerium(III) oleate, form either a mono- or a hemihydrate. The X-ray analysis showed that the neat lanthanide soaps have a lamellar bilayer structure at room temperature. The thermal behavior has been investigated by cross-polarized optical microscopy (POM), differential scanning calorimetry (DSC), and thermogravimetric analysis (TGA). POM scans showed that all the lanthanide oleates form a lamellar phase in the presence of excess water. Small-angle X-ray scattering (SAXS) and XRD were used to investigate the internal structure of the bulk lanthanide oleates in excess water, and these X-ray results confirmed that the lanthanide oleates do not swell in water. Select lanthanide oleates were dispersed in water to form nonswelling lamellar submicrometer particles, confirmed by dynamic light scattering (DLS) and synchrotron SAXS measurements. NMR results indicated that colloidal dispersions of lanthanide oleates containing paramagnetic ions, such as gadolinium(III), terbium(III), and dysprosium(III), have a significant effect on the longitudinal (T_1) and transverse (T_2) relaxation times of protons in water. Time-resolved fluorescence measurements have demonstrated that colloidal dispersions of europium(III) oleate exhibit strong luminescence. The rare earth metal soaps exemplify the potential of self-assembled chelating amphiphiles as contrast agents in medical imaging modalities such as magnetic resonance imaging (MRI) and fluorescence imaging.

Introduction

Lanthanide-containing metal soaps were first synthesized by Misra in the early 1960s,[1,2] and their applications as detergents, catalysts, optical polymer fibres, polymer stabilizers, and medical products have been the focus of an intense body of research over the past few decades.[3−6] Their mesophase behavior was, however, not discovered until 1998 for cerium(III) alkanoates.[7] It was shown that in the solid state such systems tend to adopt a lamellar bilayer structure with the chains locked into an all-trans conformation. At the melting point of the chains, the system may display a direct transition to an isotropic ionic liquid. This temperature at which an ionic liquid is formed decreases across the lanthanide series due to the effect of lanthanide contraction.[8] As the ionic radius of the lanthanide cation decreases, repulsive electrostatic interactions between the carboxylate groups become more pronounced and it is easier to break down the bilayer structure of the metal soap. However, for systems containing light Ln^{3+} ions having large ionic radii, an intermediate mesophase may be observed between the solid and liquid states.[8] This type of behavior occurs when, at the melting point of the alkyl chains, electrostatic interactions between the Ln^{3+} ions and the bridging groups are still sufficiently favorable to maintain a layer structure. The mesophase formed, viz., a smectic A liquid crystalline phase, retains the layered lamellar bilayer structure but with the loss of in-plane ordering. Such behavior is characterized by SAXS results showing the disappearance of the wide angle peak at approximately 21° ($d \approx 4.2$ Å) and the appearance of a much broader peak in the same region characteristic of disordered alkyl chains. In practice, mesophase behavior has only been observed for pure lanthanum(III), cerium(III), praseodymium(III), and neodymium(III) systems, although mesophase behavior has been observed in binary systems containing heavier lanthanide ions.[9]

The phase behavior of liquid crystalline mesophases may be broadly predicted using previously discovered "structure−property" relationships and it is possible to hone phase behavior by adjusting the coordinating amphiphile. For example, it has been shown that the amphiphile chain length has a pronounced effect on the mesophase behavior.[10] For cerium(III) alkanoates, both the smectic A phase and an unidentified highly viscous mesophase are observed at shorter chain lengths whereas only the smectic A phase was observed at longer chain lengths. Previous research has also shown that the temperature at which mesophase behavior is accessed may be lowered by introducing unsaturation or branching into the chains due to the reduction in van der Waals attraction forces in the chain region.[11−13] Here, we investigate the effect of unsaturation on phase behavior by using lanthanide metal soaps with oleate chains. We have characterized the structure and phase behavior of such soaps using elemental analysis, Fourier transfer infrared spectroscopy (FT-IR), and X-ray diffraction analysis (XRD). Their thermal behavior has been investigated by cross-polarized optical microscopy (POM), differential scanning calorimetry (DSC),

* Corresponding author. E-mail: calum.drummond@csiro.au.
[†] CSIRO Molecular and Health Technologies (CMHT).
[‡] CSIRO Materials Science and Engineering (CMSE).

10.1021/jp906344u Published 2009 by the American Chemical Society
Published on Web 11/11/2009

and thermogravimetric analysis (TGA). POM water penetration scans were used to investigate the lyotropic phase behavior of these compounds. To our knowledge, this is the first study on the self-assembly behavior of unsaturated lanthanide-containing amphiphile systems. A complementary future paper will investigate the self-assembly behavior of lanthanide-containing systems comprised of amphiphiles possessing branched hydrocarbon chains.

In addition, we investigate these systems as potential contrast agents for magnetic resonance imaging (MRI). Contrast agents, used to increase the contrast between the target organ and the surrounding tissues for MRI studies, have been in use for the past 10 years. Most contrast agents approved for human use are extracellular fluid (ECF) gadolinium-based agents such as Magnevist.[14] Gadolinium (Gd) is highly paramagnetic and significantly reduces both the longitudinal and transverse proton relaxation times (T_1 and T_2) relative to pure water.[15] As "free" gadolinium(III) is toxic, it is sequestered by chelation[16] or encapsulation[17−19] for biomedical applications. Commercial contrast agents are dominated by highly stable gadolinium complexes based on the polyaminocarboxylate ligand[20] and Magnevist is the gadolinium complex of diethylenetriaminepentaacetic acid.[14] However, these clinical contrast agents are all nonspecific and suffer from the shortcomings of limited resolution and relatively low inherent sensitivity.[21] In addition, such gadolinium-based agents have a relatively short lifetime within the vascular system, requiring repeated injections of the contrast agent. Here we investigate the incorporation of gadolinium and other lanthanide ions within an ordered nanostructured self-assembled phase allowing the paramagnetic properties of the metal ion to be potentially combined with other desirable characteristics of the phase such as drug encapsulation, controlled release, and targeted delivery.[22,23] In the case of the terbium(III) and europium(III) ions, which are luminescent in aqueous solution and generally retain their luminescence when bound to complex ligand systems, such systems could additionally be used as contrast agents for optical fluorescence imaging.[24]

We also investigate the use of submicrometer dispersions of such systems. Various nanoparticulate carrier systems for gadolinium, including silica, liposomes, perfluorocarbon (PFC) nanoparticles, and dendrimers, have been investigated previously as MRI contrast agents with the aim of increasing sensitivity and allowing the targeting of specific organ systems.[25−29] Here, we look at dispersions which are self-assembled in the solid or gel-like state, analogous to "solid lipid nanoparticles" (SLNs).[30−32] SLNs are particulate systems previously used for parenteral drug administration[32] with mean particle diameters ranging from 50−1000 nm. We found that the lanthanide metal soaps are thermodymamically stable to dispersion in excess water, and SAXS results indicate that the lamellar bilayer structure is retained within the dispersed samples. The relaxivities of these dispersions were evaluated in vitro and some were found to exhibit the characteristics of MRI contrast agents.

Results and Discussion

Lanthanum(III) (La), cerium(III) (Ce), neodymium(III) (Nd), samarium(III) (Sm), europium(III) (Eu), gadolinium(III) (Gd), terbium(III) (Tb), and dysprosium(III) (Dy) oleates were synthesized as described in the Experimental Section. Elemental analysis and FT-IR were used to verify the structure and purity of the obtained compounds. The results are in good agreement with the proposed structures.

Elemental Analysis. The elemental analysis results for C, H, lanthanide metals, and the hydration content of the synthesized lanthanide oleates are shown in Table 1, together with the molar ratio of oleic acid and lanthanide metal ions. For all the lanthanide oleates, the ratio of the oleic acid content to the lanthanide ion content was found to be 3.09 ± 0.04 ($n = 8$), acceptable within experimental error to the theoretically expected value of 3.00 for the stoichiometric $Ln(C_{17}H_{33}COO)_3$. The C, H, and Ln contents were close to the theoretically expected values from the stoichiometry $Ln(C_{17}H_{33}COO)_3$. Under the reaction conditions used here, the lanthanide oleates were typically in monohydrate or hemihydrate form with the exception of cerium(III) oleate which is anhydrous. At the moment we are unable to explain why cerium(III) oleate is the only anhydrous amphiphile in the study.

TABLE 1: Elemental Analysis of the Lanthanide Oleates

Ln oleates	% C[a]	% H[a]	% Ln[a]	oleic acid/Ln	hydration
La oleate	62.8 (64.7)	9.1 (9.8)	13.0 (13.8)	3.03	1
Ce oleate	64.7 (65.8)	10.2 (10.1)	13.6 (14.2)	3.09	0
Nd oleate	62.9 (64.3)	9.7 (9.9)	13.6 (14.3)	3.08	1
Sm oleate	63.1 (64.5)	9.8 (9.9)	13.9 (14.8)	3.07	0.5
Eu oleate	63.6 (64.4)	9.8 (9.9)	14.3 (15.1)	3.11	0.5
Gd oleate	63.4 (64.1)	9.6 (9.8)	13.8 (15.5)	3.12	0.5
Tb oleate	63.1 (64.0)	10.0 (9.9)	13.8 (15.6)	3.17	0.5
Dy oleate	63.6 (63.8)	10.0 (9.9)	14.2 (15.9)	3.05	0.5

[a] The calculated values are given in parentheses. The theoretical molar ratio of oleic acid to Ln is 3. Hydration refers to the mole content of H_2O in 1 mol of Ln oleate.

Fourier Transfer Infrared Spectroscopy. Infrared spectra in the spectral region from 400 to 4000 cm^{-1} were recorded for all the lanthanide oleates. Such vibrational spectroscopy of long-chain metal carboxylates provides information on the metal-ion carboxylate coordination, on the chain conformation, and on the packing of the alkyl chain.[33] FT-IR assignments for oleic acid, lanthanum(III) oleate, and gadolinium(III) oleate are listed in Table 2. As the FT-IR spectra for the other lanthanide oleates are very similar to that of lanthanum(III) oleate, we focus our discussion on this spectrum. The absorption maximum, characteristic of the aliphatic chain of the acid molecule, remains almost unchanged upon formation of the soap from the acid. The absorption bands of the C−H stretching vibrations, viz., the symmetrical stretching vibration of CH_2 at 2860−2850 cm^{-1}, asymmetrical stretching vibration of CH_2 at 2920 cm^{-1}, asymmetrical stretching vibration of CH_3 at 2960−2950 cm^{-1}, and deformation band of CH_3 at 1380−1080 cm^{-1}, were observed in the spectra of lanthanum(III) oleate as well as of oleic acid. The absorption bands near 2660−2650, 1700, 950−930, 690, and 550 cm^{-1} corresponding to the carboxyl group in the spectra of oleic acid have completely disappeared in the spectra of lanthanum(III) oleate.

Absorption due to OH stretching modes occurs in the range of 3500−3300 cm^{-1} and was observed for lanthanum(III) oleate as a broadband of medium intensity centered at 3450 cm^{-1}. This supports a hydrate structure for lanthanum(III) oleate or the presence of physisorbed water.[34] However, the peak at ca. 3450 cm^{-1} was not observed in the FT-IR spectrum of cerium(III) oleate, confirming the anhydrous nature of this compound as indicated by the elemental analysis results.

The complete disappearance of the C═O stretch band of the carboxyl group, and the subsequent emergence of two absorption bands corresponding to the asymmetric $\upsilon_{as}(COO^-)$ and symmetric $\upsilon_s(COO^-)$ stretches of the carboxylate moiety (COO^-) at 1545 and 1454 cm^{-1}, confirm that the conversion of oleic acid to lanthanum(III) oleate is complete and that these soaps possess an ionized structure.[35,36] Furthermore, based on previous

TABLE 2: Infrared Absorption Spectral Frequencies (cm^{-1}) with Their Assignments for Oleic Acid, Lanthanum(III) Oleate, and Gadolinium(III) Oleate

assignments		infrared absorption spectral frequencies (cm^{-1})		
		oleic acid	La oleate	Gd oleate
1	O−H stretch	3500−2500 broad	3434	3435
2	C−H stretch in C═C−H	3005	3006	3006
3	CH3, C−H asymmetric stretch	2950	2951	2949
4	CH2, C−H asymmetric stretch	2924	2923	2922
5	CH2, C−H symmetric stretch	2854	2855	2854
6	OH stretch	2674		
7	C═O stretch	1710		
8	COO−, C−O asymmetric stretch		1545	1546
9	CH2, deformation	1462		
10	COO−, C−O symmetric stretch		1457	1456
11	CH3, symmetric deformation	1378	1380	1378
12	progressive bands (CH2, twisting and wagging)	1300−1080	1350−1094	1348−1085
13	C−O stretch	1285		
14	OH, out-of-plane stretch	937		
15	CH2, rocking	724	723	723
16	COOH, bending mode	604		
17	COOH, wagging mode	482		
18	Ln−O, stretch		518	517

studies of carboxylates, the wavenumber separation ($\Delta\upsilon$), between the $\upsilon_{as}(COO^-)$ and $\upsilon_s(COO^-)$ IR bands can be used to diagnose the type of interaction between the carboxylate moiety and the metal ion.[37−39] The largest $\Delta\upsilon$ (200−320 cm^{-1}) corresponds to a monodentate interaction, the medium range $\Delta\upsilon$ (140−190 cm^{-1}) indicates a symmetric coordinative bidentate interaction, and the smallest $\Delta\upsilon$ (<110 cm^{-1}) corresponds to a multidentate interaction. For lanthanum(III) oleate, $\Delta\upsilon$ (<100 cm^{-1}) is much lower than the carboxylate stretching vibrations in alkali soaps (i.e., $\Delta\upsilon$ = 138 cm^{-1}),[40] and we propose an asymmetric multidentate coordination here.

The bands observed near 518 cm^{-1} in the spectra of lanthanum(III) oleate may be due to stretching modes of the La−O ionic bond, although further confirmation is needed to allow a more definitive assignment.[7]

^{1}H NMR. We note that the ^{1}H NMR spectra for gadolinium(III), terbium(III), and dysprosium(III) oleate contain a broad peak at 3−1 ppm, indicating that these lanthanide oleates are paramagnetic. The paramagnetic nature of the gadolinium(III), terbium(III), and dysprosium(III) oleates suggests they may possess the characteristics of an MRI contrast agent.

X-ray Powder Diffraction. Room temperature X-ray powder diffraction images were recorded for the Ln oleates (Ln = La, Ce, Nd, Sm, Eu, Gd, Tb, and Dy). All the lanthanide oleates display sharp diffraction peaks in the small-angle region indicating the presence of long-range order in the system. Representative XRD patterns (for lanthanum(III) oleate, gadolinium(III) oleate, and dysprosium(III) oleate) are shown in Figure 1.

All the diffraction patterns obtained show peaks with *d*-spacing values in the ratio 1:1/2:1/3:...:0.1/*n*. These diffraction peaks correspond to the successive (00*l*) Bragg reflections and indicate the presence of a lamellar bilayer structure. Within such a structure the polar groups of the lanthanide oleate molecules are localized in infinite, parallel, and equidistant planes. These planes are separated by a bilayer of alkyl chains. The interplanar layer *d*-spacing corresponds to the distance between two successive layers of Ln^{3+} ions and is listed in Table 3 for all samples. We note that after melting and then cooling the lanthanide oleates, fewer orders of reflection are seen in the diffraction pattern. This may reflect kinetic difficulties with reforming a partially ordered structure from the fully disordered state. Similar behavior was observed for some of the lanthanide(III) 4-alkoxybenzoates which showed mesophase behavior in the heating but not in the cooling direction.[41]

Scattering in the wide-angle region of the spectrum may be used to comment on the packing of the alkyl chains. For dysprosium(III) and terbium(III) oleate, discrete peaks are seen in the wide-angle region (approximately 20−25°), indicating fully crystalline packing with hydrocarbon chains locked into an all-trans conformation and the polar headgroups ordered into a crystalline array. As we move from right to left across the lanthanide series, for gadolinium and europium(III) oleate we note that these discrete peaks are replaced by a broad peak at approximately 21° ($d \approx 4.2$ Å) characteristic of disordered headgroups but with the chains retaining an all-trans conformation. For lanthanide oleates to the left of the series (lanthanum, cerium, neodymium, and samarium(III) oleate) we observe the disappearance of the wide-angle peak at approximately 21° and the appearance of a much more diffuse band in the same region characteristic of disordered alkyl chains and indicating the formation of a layered smectic mesophase.

For oleate chains adopting an all-trans conformation perpendicular to the metal ion base plane it is possible to calculate the maximal average *d*-spacing of the bilayer structure using the formula:

$$d_{max} = 2d_{C-H} + 2(n-2)d_{C-C}\sin 56.5° + 2d_{C=C} + 2d_{C-O} + 2r_{Ln^{3+}}$$

where *n* denotes the total number of carbon atoms, $d_{C-H} = 1.09$ Å, $d_{C-C} = 1.54$ Å, $d_{C=C} = 1.34$ Å, and $d_{C-O} = 1.36$. Here we use the ionic radii $r_{Ln^{3+}}$ values which are reported in the literature for rare-earth complexes with a coordination number of six.[42] This assumes that the unsaturated oleic acid molecules are bent at the cis double bond, and the chain axes of the two parts have equal angles of tilt 56.5° to the basal plane but tilt in opposite directions (Figure 2). Maximal average *d*-spacings calculated for all the Ln oleates are listed in Table 3. For those systems where the XRD results predict an all-trans conformation of the chains (i.e., europium(III), gadolinium(III), terbium(III), and dysprosium(III) oleate), we find that in general the experimentally determined *d*-spacings are slightly lower than those calculated (by approximately 3−7 Å) which may indicate that the chains are slightly tilted with respect to the basal plane.

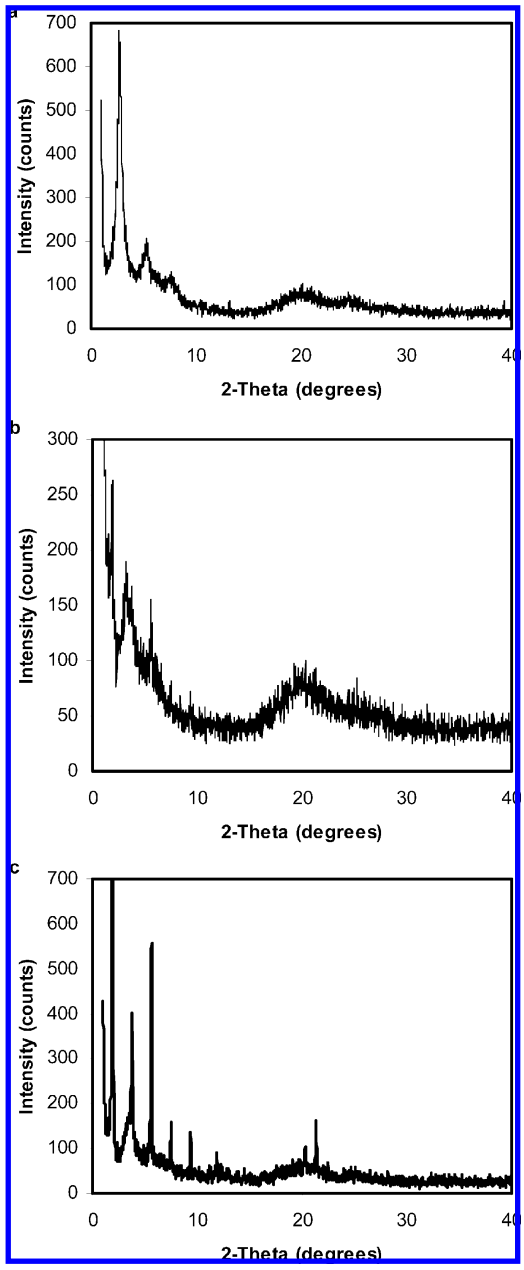

Figure 1. X-ray diffraction pattern for (a) lanthanum(III) oleate, (b) gadolinium(III) oleate, and (c) dysprosium(III) oleate at room temperature.

However, for those systems with fluid chains (lanthanum(III), cerium(III), neodymium(III), and samarium(III) oleate) as shown by XRD measurements, the calculated values are much higher than the actual bilayer spacings (by approximately 20 Å), as expected. The large decrease in *d*-spacing observed on transition from an all-trans conformation of the hydrocarbon chain to a fluid conformation reflects the increase in trans−gauche rotational isomerism with fluid chains.

These XRD results indicate that mesophase behavior is seen only for those lanthanide ions to the left of the lanthanide series (i.e., lanthanum(III), cerium(III), neodymium(III), and samarium(III) oleate) with the formation of a layered smectic mesophase at room temperature. The narrowing of the temperature range over which mesophase behavior is observed as the lanthanide series is traversed has been previously observed for lanthanide alkanoates.[8] A detailed explanation for this behavior has been provided in the Introduction.

Thermal Behavior of Neat Lanthanide Oleates. It was not easy to obtain a good diagnostic texture of the neat lanthanide oleate materials by cross-POM. Lanthanide oleates have a very high viscosity and are not very fluid even at high temperatures. Figure 3 shows the cross-POM image for pristine lanthanum(III) oleate and gadolinium(III) oleate at room temperature. The texture had a grainy appearance characteristic of a lamellar-type structure. When cooling the lanthanide oleates from a molten state to room temperature, no immediate crystallization was observed with cross-POM. However, a lamellar-type structure formed after leaving the systems for some time with the time of formation dependent on the final structure. It was found from cross-POM that the lamellar to isotropic liquid melting points of the lanthanide oleates decrease over the lanthanide series from lanthanum to dysprosium (Table 4), reflecting the influence of the ion size on the melting point.[8] Note that we use the term melting point to describe the temperature at which the system forms an isotropic liquid regardless of whether the preceding phase is crystalline or a smectic mesophase. In the literature this is sometimes described as the clearing point.

Melting points for the lanthanide oleates were confirmed by DSC scans over the range of −150 to +150 °C at a heating rate of 2.5 °C min^{-1} and are listed in Table 4. The melting points obtained by visual inspection were similar to those recorded by DSC, and a decrease in melting point is observed across the lanthanide series. This may be explained by consideration of the lanthanide ion size: the smaller the lanthanide ion, the more unstable the layer structure becomes, and hence less thermal energy is required to break down the lamellar packing. DSC scans for dysprosium(III), gadolinium(III), and lanthanum(III) oleate (representing a crystalline, gel, and smectic phase at room temperature, respectively) were also run at 15 °C min^{-1} (which allows easier visualization of the melting point peaks) and are shown in Figure 4. Transition temperatures seen for these scans are higher than those listed in Table 4, reflecting an artifact of the increased heating rate. We look first at the curve for dysprosium(III) oleate (Figure 4c) which forms a fully crystalline structure at room temperature as evidenced by the SAXS and XRD data. A large endothermic peak observed at ca. 44 °C represents the crystal−fluid melting transition. A much smaller endothermic peak at around −78 °C may reflect a crystal−crystal transition within the system, perhaps involving a tilt of the hydrocarbon chains. For gadolinium(III) and lanthanum(III) oleate (Figure 4, b and a) which form gel and fluid phases at room temperature, the endothermic melting point is associated with a much smaller enthalpy change than that for dysprosium(III) oleate as these already have fluid headgroups (gadolinium(III) oleate) and fluid headgroup and chain regions (lanthanum(III) oleate). A second endothermic peak seen at much lower temperatures (−72 °C for gadolinium(III) oleate and −59 °C for lanthanum(III) oleate) probably marks the crystal−gel and crystal−smectic transitions. Except for cerium(III) oleate, water loss peaks are observed for all samples at approximately 110−120 °C.

The relatively high temperature behavior of the lanthanide oleates was also investigated by TGA. The general decomposition pathway for lanthanide soaps is considered to be

$$2Ln(CH_3(CH_2)_nCOO)_3) \xrightarrow{\text{heating}} Ln_2O_3 + 3(CH_3(CH_{2n}CO(CH_2)_nCH_3) + 3CO_2$$

TABLE 3: *d*-Spacings of Lanthanide Oleate Samples, Neat, in Excess Water, or Dispersed as Submicrometer Particles in Water[a]

	d-spacing (Å)				
Ln oleates	calcd	XRD (neat)	XRD (excess water)	SAXS (excess water)	SAXS (dispersions)
La oleate	50.8	32.0	–	–	–
Ce oleate	50.7	32.6	–	–	–
Nd oleate	50.6	29.9	–	–	–
Sm oleate	50.6	27.3	–	–	–
Eu oleate	50.6	43.2	43.4	44.7	45.9
Gd oleate	50.5	47.4	47.5	46.9	46.4
Tb oleate	50.5	46.4	47.2	46.0	46.5
Dy oleate	50.5	45.9	46.2	44.9	45.6

[a] All measurements were carried out at room temperature using XRD or SAXS. Measurements of the *d*-spacings for lanthanum, cerium, neodymium, and samarium(III) oleate in excess water were not determined.

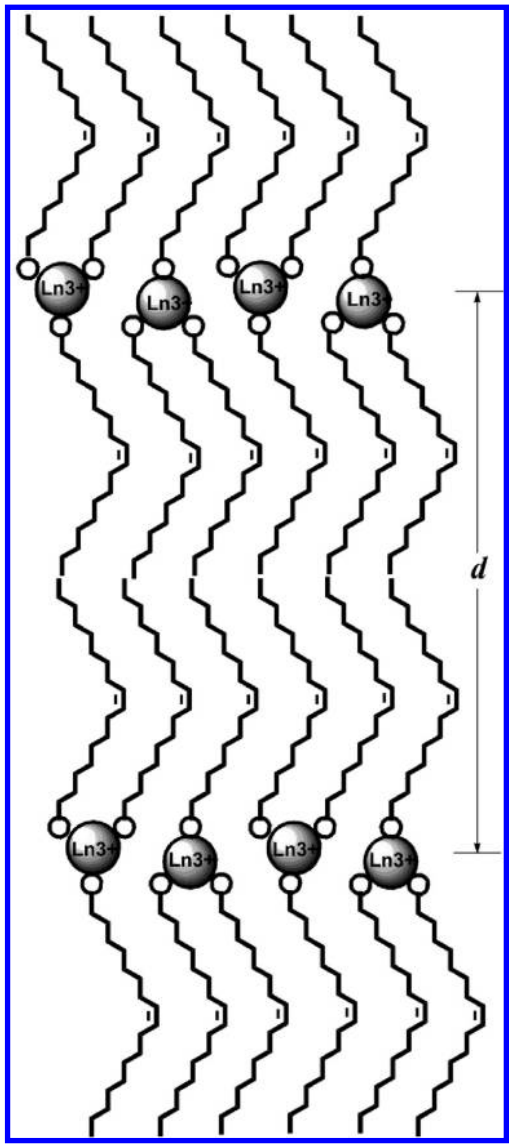

Figure 2. Schematic representation of the lanthanide oleate bilayer structure with the chains in an all-trans crystalline conformation.

In the TGA trace of air-stored lanthanide soaps, the dehydration of physisorbed water happens around 100 °C.[43] Decomposition to volatiles such as alkanones and CO_2, basic soaps, metal oxycarbonates, and metal oxides usually began around 200 °C. The TGA curves for all lanthanide oleates are very similar except cerium(III) oleate. For cerium(III) oleate, there is no H_2O loss peak at around 120 °C, further indicating cerium(III) oleate is not hydrated. Figure 5 shows the TGA curve for lanthanum(III) oleate. The onset of chemical degradation was marked by discolouration and obvious weight loss. The weight loss continued until the sigmoidal trace flattened to close to the predicted oxide weight at about 550−600 °C. The TGA trace of lanthanum(III) oleate showed dehydration of physisorbed water between about 100 and 150 °C and a clear division of the carboxylate chain decomposition into three weight loss events between 200 and 550 °C. The first step after water removal may be due to the cleavage of the methyl carbon chain and the carboxylate chain between two lanthanum(III) oleate molecules to form the oxygen bridged dilanthanum tetracarboxylate. The majority of the weight loss happened at step two (380−460 °C). The third change (460−550 °C) presumably corresponded to the decomposition of lanthanum oxycarbonate to lanthanum oxides and CO_2. It was found that one water molecule was adsorbed per lanthanum(III) oleate chelating amphiphile, i.e., a 1.6% weight loss which is consistent with the moisture content from the elemental analysis. The TGA traces of the other lanthanide oleates are very similar to that of lanthanum(III) oleate and are not further discussed here.

Cross-Polarized Microscopy of Lanthanide Oleates in Excess Water. Neat lanthanide oleates were melted on a glass microscopy slide, cooled to room temperature, and then exposed to water. Lanthanide oleates exhibit supercooling, and cross-POM showed that a birefringent texture developed slowly at room temperature, frequently through a fingering mechanism. The texture was consistent with the formation of an anisotropic lamellar phase. As the samples are basically nonswelling, we believe that water is not actually penetrating the sample, instead the lamellar phase crystallizes at the oleate/water interface and grows slowly into the melted sample. The lamellar phase formed most quickly (within hours) for gadolinium(III), terbium(III), and dysprosium(III) oleate (Figure 6b). For europium(III) and samarium(III) oleate, the lamellar phase formed overnight while for the remaining lanthanide oleates a week of water contact was required (Figure 6a). It seems that ease of formation is strongly dependent on the structure of the neat material with the speed of formation of a particular phase in water, increasing in the order smectic < gel-like < crystalline. A kinetically hindered reformation of the lamellar phase on cooling has implications for the dispersion process which involves emulsifying the lanthanide oleates above their melting point and then allowing them to cool. However, SAXS results on the dispersed samples discussed in the next section confirm that the lamellar structure is retained after the dispersion process.

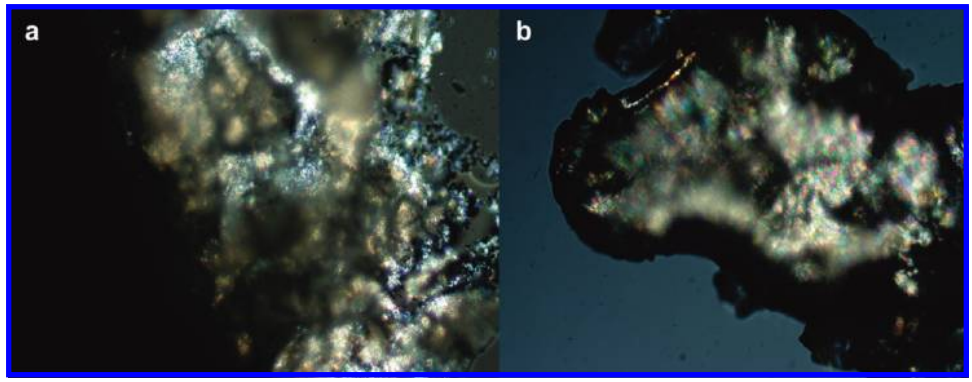

Figure 3. Cross-polarized optical microscopy images for (a) lanthanum(III) oleate and (b) gadolinium(III) oleate at room temperature.

TABLE 4: Transition Temperatures of the Lanthanide Oleates As Determined by DSC Measurements[a]

Ln oleates	T_m (°C)	T_p (°C)
La oleate	53	−60
Ce oleate	50	−60
Nd oleate	47	−65
Sm oleate	42	−70
Eu oleate	40	−75
Gd oleate	37	−80
Tb oleate	35	−80
Dy oleate	30	−80

[a] T_m refers to the temperature at which the system forms an ionic liquid. T_p refers to a low-temperature transition.

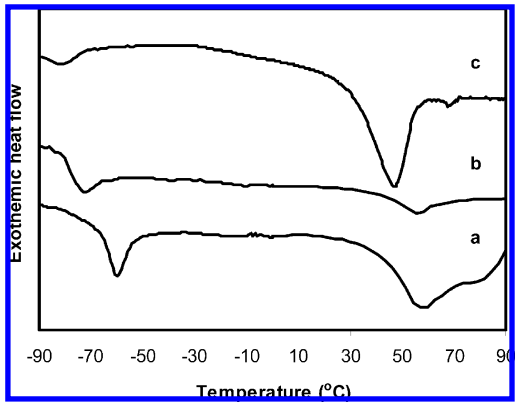

Figure 4. DSC curve for (a) lanthanum(III) oleate, (b) gadolinium(III) oleate, and (c) dysprosium(III) oleate at the heating rate of 15 °C min^{-1}.

SAXS and XRD of Lanthanide Oleates in Excess Water. Dispersions of europium(III) oleate, gadolinium(III) oleate, terbium(III) oleate, and dysprosium(III) oleate were formed and will be described more fully in the subsequent section. For these lanthanide oleates SAXS and XRD were used to investigate the structure of the bulk lanthanide oleates in excess water. Figure 7 shows the SAXS patterns for bulk europium(III) oleate, gadolinium(III) oleate, terbium(III) oleate, and dysprosium(III) oleate left in excess water for over a week. For these lanthanide oleates, one distinct scattering peak was observed with a *d*-spacing of approximately 46 Å. This lattice parameter, combined with the polarizing microscopy results, is consistent with the formation of a lamellar structure. The second-order reflection from such a structure would lie outside the accessible *q* range. For comparison, XRD data were also collected for neat solid Ln (Ln = Eu, Gd, Tb, and Dy) oleates, and bulk Ln (Ln = Eu, Gd, Tb, and Dy) oleates left in excess water for over a week. The XRD spectra show a number of reflections consistent

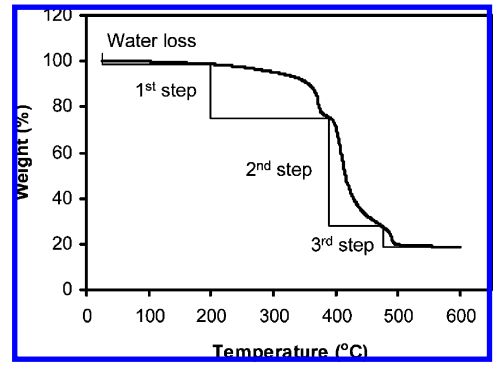

Figure 5. TGA trace for lanthanum(III) oleate.

with the retention of the lamellar structure seen for the neat samples. Table 3 lists the *d*-spacing results obtained from both XRD and SAXS measurements for neat samples and those in excess water. We note that the *d*-spacing of the lanthanide oleates has remained unchanged after a week of water exposure, indicating that these lanthanide oleates do not swell in water, and they belong to the class of nonswelling soaps.

Dispersions of Lanthanide Oleates. The paramagnetic nature of gadolinium(III), terbium(III), and dysprosium(III) oleate, combined with their tendency to self-assemble into a nanostructured lamellar phase under excess water conditions at room temperature, suggests a potential use for such systems as contrast agents for magnetic resonance imaging. Here we have successfully dispersed these systems into submicrometer-sized colloid particles using the methods described in the Experimental Section and show that they form stable colloidal dispersions of self-assembled amphiphiles. In addition, the dispersed phase of europium(III) oleate has been investigated. The particle size distributions (D_{10}, D_{50}, D_{90}) for these dispersions are provided in Table 5.

SAXS experiments were carried out on the dispersed samples to confirm that long-range structural order is present and to obtain accurate *d*-spacings. Due to the weak scattered intensity typically obtained from dispersions, experiments were carried out at a synchrotron radiation facility as described in the Experimental Section. Samples were run at 25 °C for comparison with previous SAXS and XRD data on the bulk samples and at 37 °C for physiological relevance. At 25 °C all samples showed a well-defined peak in the SAXS pattern, Figure 8, indicating that long-range order is retained in the dispersed samples. Calculated *d*-spacings for the dispersions (Table 3) are in close agreement with previous results on the corresponding bulk samples strongly suggesting that the systems have retained the bilayer structure in the dispersed phase. We note that gadolinium(III) oleate and terbium(III) oleate display only

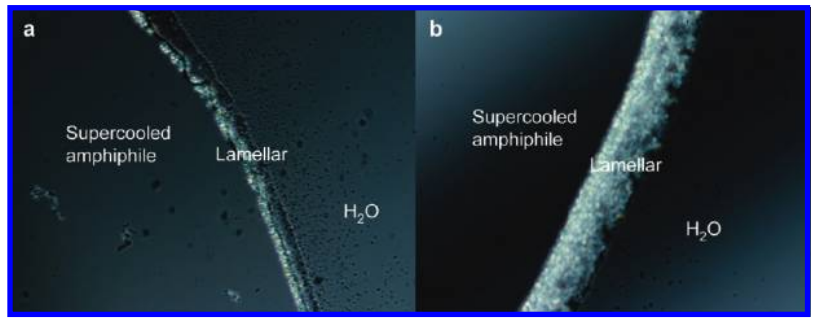

Figure 6. (a) Lanthanum(III) oleate and (b) gadolinium(III) oleate in excess water viewed with cross polarized optical microscopy recorded at 25 °C. The sample was melted and then cooled to room temperature prior to water exposure.

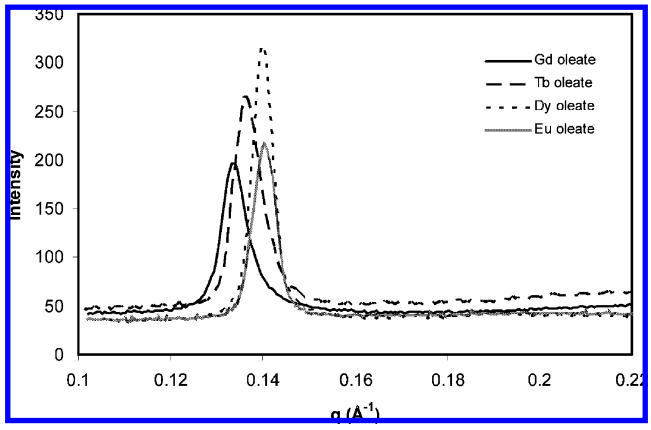

Figure 7. SAXS profiles for bulk Ln oleates (Ln = Eu, Gd, Tb, and Dy) exposed to excess water.

TABLE 5: Relaxivities of the Lanthanide Oleates at 0.47 T (20 MHz) and Room Temperature

	particle size (nm)			relaxivity (mM^{-1} s^{-1})	
dispersions	D_{10}	D_{50}	D_{90}	r_1	r_2
Eu oleate	160	420	910	0.04	0.20
Gd oleate	280	530	1160	2.78	6.46
Tb oleate	250	650	1120	0.06	7.47
Dy oleate	260	600	1180	0.09	6.59
Magnevist	–	–	–	4.90	6.26

a weak diffraction peak at 37 °C and dysprosium(III) oleate and europium(III) oleate no diffraction at all. For gadolinium(III) oleate and terbium(III) oleate a small decrease in lattice parameter is seen at the higher temperature. Gadolinium(III), dysprosium(III), and terbium(III) oleate all have melting points at or below 37 °C, and we would expect loss of the bilayer structure in the dispersed samples. Where weak diffraction is seen, this probably reflects a residual thermodynamically unstable sample. Although europium(III) oleate has a melting point slightly higher than 37 °C, no diffraction was seen for this sample.

Relaxivity of Lanthanide Oleate Dispersions. The lanthanide oleate dispersions were evaluated for their ability to modify the relaxation rate of water in vitro using a standard NMR spectrometer at 20 MHz and room temperature. Typical plots to obtain longitudinal (r_1) and transverse (r_2) relaxivities for gadolinium(III) oleate are shown in Figure 9 with a full listing of the relaxivity data in Table 5. As a comparison, data determined by us for the commercial MRI contrast agent Magnevist has been included. We show that the gadolinium(III) oleate dispersion significantly reduces the relaxation time (T_1 and T_2) relative to pure water ($T_1 = T_2 = 2$ s), and that the relaxation rate increases linearly with the concentration of gadolinium(III) oleate (Figure 9). Terbium and dysprosium(III) oleate, while significantly reducing the transverse proton relaxation time, have very long longitudinal relaxation times.

Although the longitudinal relaxivity of gadolinium(III) oleate (2.78 mM^{-1} s^{-1}) is much higher than that of the other lanthanide oleates, it is slightly lower than that of Magnevist (4.90 mM^{-1} s^{-1}) under the same conditions. The transverse relaxivity of gadolinium(III) oleate (6.46 mM^{-1} s^{-1}) is very similar to that of terbium(III) oleate, dysprosium(III) oleate, and Magnevist (6.26 mM^{-1} s^{-1}). As expected, both the longitudinal and transverse relaxivities for europium(III) oleate, which is not paramagnetic, are very small.

We note that reaction equilibria constants in the interfacial microenvironment of amphiphile self-assembly materials can be markedly different from bulk solution values.[44] Consequently, it is difficult to make a priori predictions of the chelation constants for the self-assembled lanthanide oleates. In this report, we demonstrate the potential of the class of self-assembled chelating amphiphiles, as medical imaging agents, without focusing on possible in vivo transmetalation issues. Transmetalation will be the subject of future work on chelating self-assembled amphiphiles.

The relatively high relaxivities of gadolinium(III), terbium(III), and dysprosium(III) oleates, comparable to those of the commercially available agent, Magnevist, combined with their ability to form submicrometer particles exemplifies the potential of this form of ordered nanostructured self-assembly colloids as MRI contrast agents.

Luminescent Behavior of Europium(III) Oleate. While europium(III) oleate is a poor MRI contrast agent compared to gadolinium(III), terbium(III), and dysprosium(III) oleates, it has luminescent properties. The fluorescence excitation and emission spectra of europium(III) oleate particle dispersions are displayed in Figure 10, with excitation and emission spectra very close to the typical excitation and emission wavelength for europium(III) ions.[24,45] A time-resolved study with excitation at 300 nm and detection of emission at 620 nm was used to investigate the time-resolved properties of europium(III) oleate particle dispersions in water. The quenching of fluorescence in aqueous systems due to the direct coordination of water molecules to the europium(III) complex and radiationless energy transfer from excited states to the aqueous solvent shell, is the common limitation of europium(III) ion based detection of bioanalytes.[24,45] Here it was found that europium(III) oleate retains luminescent properties after dispersion. Figure 11 shows the plot of fluorescence response versus europium(III) oleate concentration. The fluorescence response increased monotonically with the concentration of europium(III) oleate, with a detection limit of ca. 1.8×10^{-10} M suggesting some potential

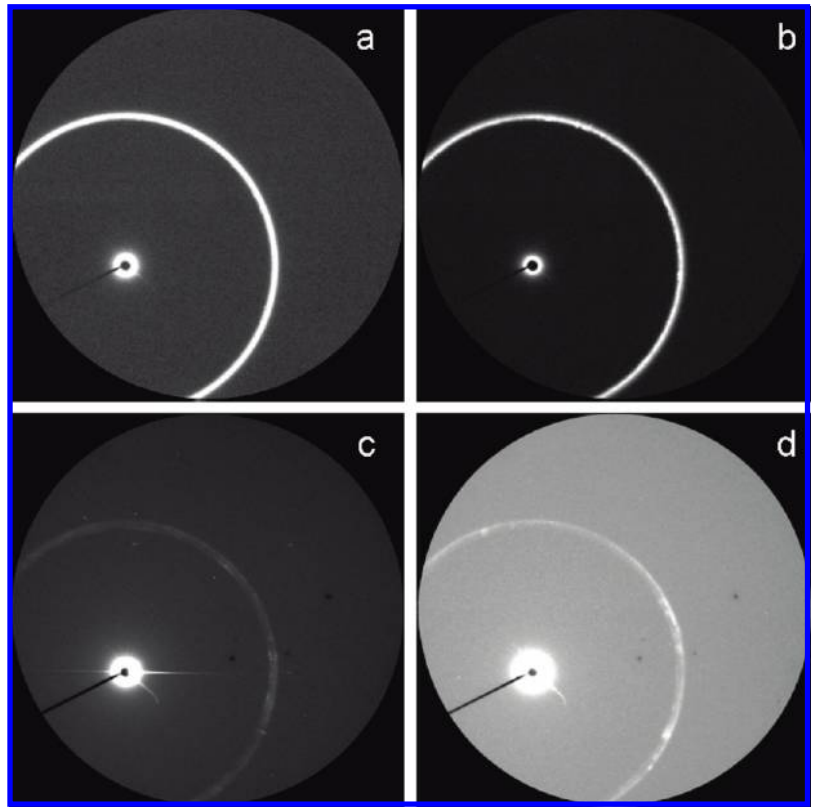

Figure 8. SAXS images for colloidal dispersions of (a) europium(III) oleate, (b) gadolinium(III) oleate, (c) terbium(III) oleate, and (d) dysprosium(III) oleate.

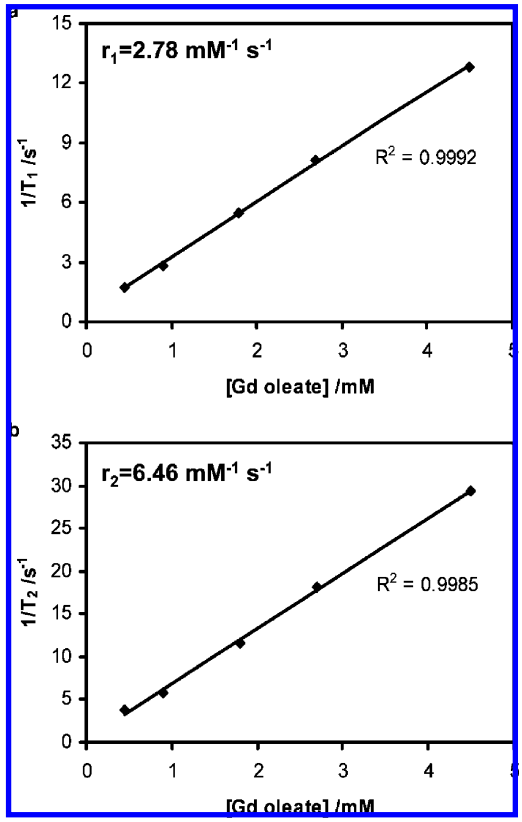

Figure 9. Plot of proton (a) longitudinal relaxivity r_1 and (b) transverse relaxivity r_2 at 20 mMz and room temperature with a MINISPEC from Bruker vs the concentration of gadolinium(III) oleate.

for this self-assembled amphiphile material type as a contrast agent for fluorescence imaging.

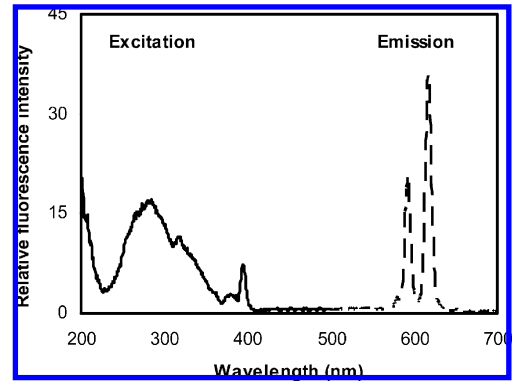

Figure 10. Fluorescence excitation spectrum and fluorescence emission spectrum of a europium(III) oleate particle dispersion in water.

Conclusions

We have synthesized the Ln oleates (Ln = La, Ce, Nd, Sm, Eu, Gd, Tb, and Dy), with a stoichiometry corresponding to $Ln(C_{17}H_{33}COO)_3 \cdot nH_2O$. A combination of elemental, thermogravimetric, spectroscopic, and calorimetric data showed that the synthesized lanthanide oleates, except for cerium(III) oleate, have a preference for hydrate formation. X-ray diffraction showed that these metallic soaps consist of a lamellar lanthanide oleate structure at room temperature. The melting points of the lanthanide oleates decreased on traversing the lanthanide series, ranging from 53 °C for lanthanum(III) to 30 °C for dysprosium(III) oleate. Cross-polarized optical microscopy, XRD and SAXS results showed that the lamellar liquid crystalline structure is nonswelling in excess water. The lanthanide oleates can be dispersed in water to form submicrometer nonswelling colloidal particles. The proton relaxivity for the dispersed particles of

these lanthanide oleates was investigated by NMR in vitro. It was found that gadolinium(III) oleate can significantly reduce the relaxation rate relative to pure water. The longitudinal proton relaxivity of gadolinium(III) oleate is slightly lower than that of the commercial MRI contrast agent, Magnevist, while the transverse relaxivity is similar. NMR studies have demonstrated that terbium and dysprosium(III) oleate are also paramagnetic, and that they display higher transverse relaxivities than Magnevist. We have therefore exemplified the potential of nonswelling self-assembly colloids as MRI contrast agents. In addition, europium(III) oleate illustrated the possibility that such systems could serve as fluorescent contrast agents for medical imaging. Dispersions of nonswelling self-assembly colloids also have potential as multifunctional medical materials by incorporating bioactive molecules in the nanostructured self-assembly phase; a matrix with promise for encapsulation and controlled release.

Experimental Section

Materials and Instrumentation. All chemicals were used as received, without further purification. Analytical grade solvents were used for recrystallization and washing of the soaps (water contents: ethanol <0.2%; 1-pentanol < 0.2%; acetone <0.3%). Oleic acid (≥99.0% purity) was obtained from Fluka. Lanthanide chloride hexahydrate was purchased from Sigma-Aldrich. ^{1}H NMR spectra were obtained using a Bruker AV400 (400 MHz) spectrometer with deuterated chloroform as the solvent. The carbon and hydrogen contents of the Ln oleates (Ln = La, Ce, Nd, Sm, Eu, Gd, Tb, and Dy) were determined by C/H elemental microanalysis (combustion analysis) at the University of Otago, New Zealand. Rare earth metal content was determined using a Varian Vista spectrophotometer with inductively coupled plasma atomic emission spectroscopy (ICP-AES). Samples for ICP-AES analysis were prepared by dissolving 0.1 g of Ln oleate in 0.1 M HCl (15 mL). The solution was extracted with diethyl ether (3 × 30 mL) to remove the oleic acid, made up to 100 mL with Milli-Q water and used directly for ICP-AES analysis. To determine the oleic acid content, the combined diethyl ether extracts containing oleic acid were washed with saturated brine (3 × 350 mL) and the solvent removed under reduced pressure. The collected oleic acid was characterized by ^{1}H NMR and its concentration determined by titration with NaOH solution using phenolphthalein as an indicator. FT-IR spectra were obtained using a BOMEN MB 101 spectrometer (Extech Equipment Pty. Ltd.). Spectra of the crystalline samples as KBr pellets were obtained at room temperature in the 4000−400 cm^{-1} range and accumulated for 32 scans at a resolution of 8 cm^{-1}. DSC measurements under nitrogen were performed on a Mettler 3000 system. An indium standard was used to calibrate the DSC temperature (±0.3 °C) and enthalpy scale. TGA on a microbalance was carried out in the temperature range of 25−600 °C using a Mettler Toledo 851 system under a nitrogen atmosphere. A Bruker D8 Advanced X-ray Diffractometer with Cu Kα radiation (40 kV, 40 mA) monochromatized with a graphite sample monochromator was employed to determine the XRD patterns. Each sample was scanned over the 2-θ range 1−40° with a step size of 0.02° and a count time of 4 s per step. Analyses were performed on the collected XRD data for each sample using the Bruker XRD search match program EVA. Crystalline phases were identified using the ICDD-JCPDS powder diffraction database. Optical textures were observed with an Olympus IMT-2 cross-polarized optical microscope equipped with a Mettler FP82HT hot stage and a FP90 programmable temperature-controller. For these samples, neat lanthanide oleates were melted between a microscope slide and coverslip and then cooled to room temperature. Water added at the edge of the coverslip is drawn between the two glass surfaces and surrounds the solidified material by capillary action. SAXS spectra were obtained using point collimated Cu Kα radiation on a Bruker "nanostar" SAXS camera equipped with a photon sensitive 2-D "Hi-Star" detector. Experiments were performed under vacuum or under a helium atmosphere to minimize background scattering. SAXS experiments were also preformed on dispersed samples. As diffraction from such samples tends to be weak, data were collected at the 15-ID-D (ChemMatCARS) beamline of the Advanced Photon Source, Argonne, IL.[46] The experiments used a beam of wavelength λ = 1.50 Å (8.27 keV) with dimensions 200 μm × 100 μm and a typical flux of 1 × 10^{12} photons/s. 2-D diffraction images were recorded on a Bruker 6000 CCD detector with an active area of 94 × 94 mm^2 and a pixel size of 92 μm. The CCD detector was offset from the main beam allowing analysis in the q-range 0.0187−0.807 Å^{-1} at a sample to detector distance of 0.6 m. Temperature control was in the range 7−90 °C. Image analysis was carried out using AXcess, an IDL-based software package developed by Dr. Andrew Heron at Imperial College London.[47] Fluorescence excitation and emission spectra for europium(III) oleate particle dispersions were measured on a Perkin-Elmer Model LS-50B fluorimeter (cutoff filter, 430 nm; slit width, 10 nm). The optical time-resolved properties of europium(III) oleate particle dispersions were investigated by a time-resolved fluorimeter (PHERAstar, BMGLABTECH) with excitation at 300 nm and detection of emission at 620 nm. Measurements were performed in 96-well microliter plates. Background counts were 500−600, and were subtracted from sample readings. For particle dispersions of lanthanide oleates (Ln = Eu, Gd, Tb, and Dy), the longitudinal and transverse relaxation time, T_1 and T_2, were measured at 20 MHz (0.47 T) and room temperature with a MINISPEC (Bruker). For T_1 measurements, the standard inversion−recovery (IR) method was used as the pulse sequence.[48] The recycle delay time was set to 5 times the T_1 value. Typically 20 points were taken for each T_1 measurement. For T_2 measurements, the Carr−Pucell−Meiboom−Gill (CPMG) method was used.[48] The longitudinal relaxivity, r_1, and transverse relaxivity, r_2, were then determined from the slope of the linear regression fits of $1/T_1$ and $1/T_2$ vs the gadolinium concentration, respectively.

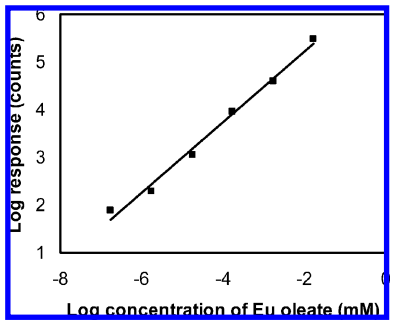

Figure 11. Fluorescence response curve of a europium(III) oleate particle dispersion in water. A linear fit has been added as a guide to the eye.

Synthesis. The synthesis of Ln(III) (Ln = La, Ce, Nd, Sm, Eu, Gd, Tb, and Dy) oleates is based on a two-step precipitation method as shown in the following equations:[49]

$$C_{17}H_{33} - COOH + NaOH \rightarrow C_{17}H_{33} - COO^{-}Na^{+} + H_2O$$

$$3C_{17}H_{33} - COO^{-}Na^{+} + LnCl_3 \rightarrow (C_{17}H_{33} - COO^{-})_3Ln^{3+} + 3NaCl$$

Specifically, oleic acid (1.448 g, 5.1 mmol) was dissolved in 1:1 ethanol/water (20 mL) with stirring at 50 °C in a water bath. To the stirring oleic acid solution, an equivalent amount of 0.5 M NaOH was added dropwise to convert the oleic acid to Na oleate. After complete addition of the NaOH, the mixture was left to stir for another 30 min at 50 °C to obtain a Na oleate solution. The solution of Na oleate solution was then added dropwise with stirring to the solution of lanthanide chloride hexahydrate (1.8 mmol), which was dissolved in 1:1 ethanol/water (20 mL), at room temperature. The addition of Na oleate solution resulted in a white precipitate. After completely adding the Na oleate solution, the mixture solution was left to stir for another 1 h at room temperature. The precipitate was then filtered and washed with hot water (3 × 50 mL), cold ethanol (3 × 50 mL), and acetone (3 × 50 mL).

The lanthanide oleates are hygroscopic, with the exception of cerium(III) oleate. The solubility of the lanthanide oleates in water is extremely low. Their solubilities in organic solvents such as acetonitrile, methanol, ethanol, 1-propanol, 1-pentanol, hexane, cyclohexane, toluene, chloroform, dichloromethane, tetrahydrofuran (THF), pyridine, DMSO, diethyl ether, and dioxane were also tested. None of these organic solvents were found to be good dissolution media for the lanthanide oleates at room temperature. At elevated temperatures, the lanthanide oleates proved to be fairly soluble in 1-pentanol, toluene, chloroform, and THF. It was found experimentally that 1-pentanol gave a better crystalline precipitate and that the lanthanide oleates separate from the other solvents as a gel, consistent with published results on fatty acid metal salts.[50] In this study a 1-pentanol/ethanol mixture (5:1) was selected as the crystallization solvent. The precipitate was collected and washed with ethanol and dried under vacuum at 40 °C for 12 h followed by freeze-drying for 24 h. Lanthanum oleate was obtained as a white powder. All the other lanthanide oleates were prepared by the same method and take on the characteristic color of the corresponding trivalent lanthanide ion.[51]

Oleic Acid. ^{1}H NMR (400 MHz, $CDCl_3$, T = 298 K): δ [ppm] 5.33−5.36 (m, 2H, $-CH{=}CH-$), 2.33−2.37 (m, 2H, $-CH_2-COO^-$), 1.97−2.02 (t, 4H, $-CH_2-CH{=}CH-CH_2-$), 1.60−1.65 (m, 2H,$-CH_2-CH_2-COO^-$), 1.27−1.31 (m, 20H, remaining CH_2), 0.86−0.90 (t, 3H, CH_3-).

Dispersion Procedures. The Ln oleates (Ln = Eu, Gd, Tb, and Dy) were dispersed in water to form particles. First, the lanthanide oleates were dissolved slowly in the minimum amount of 2-methyl-2-propanol at 60 °C to form a homogeneous solution. This was followed by the addition of 10 w/w % of the stabilizer Pluronic F127. The mixture of lanthanide oleate and F127 was added to 50 mL Milli-Q water with mixing under ultratarrax (Polytron PT 10−35 GT, Kinematica, Switzerland) for 5 min with a speed of 15,000 rpm at 80 °C. The dispersion was immediately passed through a high pressure homogenizer (Avestin, Germany) using pressures of 10000 psi for 6 passes at 60 °C. The solution appeared milky, indicating the formation of colloidal particles. The particles were sized by dynamic light scattering measurement (Coulter LS230 particle size analyzer).

Acknowledgment. C.J.D. is the recipient of an Australian Research Council Federation Fellowship. The authors thank Dr. Irena Krodkiewska (CMHT) for useful discussions and providing experimental assistance. In addition, they thank Dr. David Cookson and Dr. Robert Knott for their assistance with experiments carried out at the ChemMatCARS beamline, sector 15 at the Advanced Photon Source. Use of the ChemMatCARS sector 15 at the Advanced Photon Source was supported by the Australian Synchrotron Research Program, which is funded by the Commonwealth of Australia under the Major National Research Facilities Program. ChemMatCARS Sector 15 is principally supported by the National Science Foundation/Department of Energy under grant no. CHE-0535644. Use of the Advanced Photon Source was supported by the U.S. Department of Energy, Office of Science, Office of Basic Energy Sciences, under Contract No. DE-AC02-06CH11357.

References and Notes

(1) Misra, S. N.; Misra, T. N.; Mehrotra, R. C. *J. Inorg. Nucl. Chem.* **1963**, *25*, 195.
(2) Misra, S. N.; Misra, T. N.; Mehrotra, R. C. *J. Inorg. Nucl. Chem.* **1963**, *25*, 201.
(3) Hussain, R.; Mohammad, D. *J. Chem. Soc. Pak.* **1994**, *16*, 225.
(4) Oehme, A.; Gebauer, U.; Gehrke, K.; Lechner, M. D. *Angew. Makromol. Chem.* **1996**, *235*, 121.
(5) Zhang, Q. J.; Ming, H.; Zhai, Y. *J. Appl. Polym. Sci.* **1996**, *62*, 887.
(6) Dobetti, L.; Esposito, P.; Boltri, L. *Eur. J. Pharm. Biopharm.* **1994**, *40*, 161.
(7) Marques, E. F.; Burrows, H. D.; Miguel, M. D. *J. Chem. Soc.* **1998**, *94*, 1729.
(8) Binnemans, K.; Jongen, L.; Gorller-Walrand, C.; D'Olieslager, W.; Hinz, D.; Meyer, G. *Eur. J. Inorg. Chem.* **2000**, 1429.
(9) Jongen, L.; Hinz, D.; Meyer, G.; Binnemans, K. *Chem. Mater.* **2001**, *13*, 2243.
(10) Jongen, L.; Binnemans, K.; Hinz, D.; Meyer, G. *Mater. Sci. Eng. C—Biol. Sci.* **2001**, *18*, 199.
(11) Attard, G. S.; West, Y. D. *Liq. Cryst.* **1990**, *7*, 487.
(12) Corkery, R. W. *Phys. Chem. Chem. Phys.* **2004**, *6*, 1534.
(13) Maldivi, P.; Bonnet, L.; Giroudgodquin, A. M.; Ibnelhaj, M.; Guillon, D.; Skoulios, A. *Adv. Mater.* **1993**, *5*, 909.
(14) Pfeiffer, H.; Speck, U.; Renneke, F.; Hoyer, G.; Weinmann, H.; Rosenberg, D.; Gries, H.; Mutzel, W.; Muetzel, W. NMR, X-ray, and ultrasonic diagnostic compositions - containing salts of metal complexes, including new compounds. Patent DK8705884-A, May 29, 1988.
(15) Meade, T. J.; Taylor, A. K.; Bull, S. R. *Curr. Opin. Neurobiol.* **2003**, *13*, 597.
(16) Caravan, P.; Ellison, J. J.; McMurry, T. J.; Lauffer, R. B. *Chem. Rev.* **1999**, *99*, 2293.
(17) Bolskar, R. D.; Benedetto, A. F.; Husebo, L. O.; Price, R. E.; Jackson, E. F.; Wallace, S.; Wilson, L. J.; Alford, J. M. *J. Am. Chem. Soc.* **2003**, *125*, 5471.
(18) Kato, H.; Kanazawa, Y.; Okumura, M.; Taninaka, A.; Yokawa, T.; Shinohara, H. *J. Am. Chem. Soc.* **2003**, *125*, 4391.
(19) Sitharaman, B.; Kissell, K. R.; Hartman, K. B.; Tran, L. A.; Baikalov, A.; Rusakova, I.; Sun, Y.; Khant, H. A.; Ludtke, S. J.; Chiu, W.; Laus, S.; Toth, E.; Helm, L.; Merbach, A. E.; Wilson, L. J. *Chem. Commun.* **2005**, 3915.
(20) Weinmann, H. J.; Ebert, W.; Misselwitz, B.; Schmitt-Willich, H. *Eur. J. Radiol.* **2003**, *46*, 33.
(21) Aime, S.; Cabella, C.; Colombatto, S.; Crich, S. G.; Gianolio, E.; Maggioni, F. *J. Magn. Reson. Imaging* **2002**, *16*, 394.
(22) Malmsten, M. *Soft Matter* **2006**, *2*, 760.
(23) Drummond, C. J.; Fong, C. *Curr. Opin. Colloid Interface Sci.* **1999**, *4*, 449.
(24) Richardson, F. S. *Chem. Rev.* **1982**, *82*, 541.
(25) Sharma, P.; Brown, S. C.; Walter, G.; Santra, S.; Scott, E.; Ichikawa, H.; Fukumori, Y.; Moudgil, B. M. *Adv. Powder Technol.* **2007**, *18*, 663.
(26) Kamaly, N.; Kalber, T.; Ahmad, A.; Oliver, M. H.; So, P. W.; Herlihy, A. H.; Bell, J. D.; Jorgensen, M. R.; Miller, A. D. *Bioconjug. Chem.* **2008**, *19*, 118.
(27) Caravan, P. *Chem. Soc. Rev.* **2006**, *35*, 512.

(28) Lanza, G. M.; Abendschein, D. R.; Yu, X.; Winter, P. M.; Karukstis, K. K.; Scott, M. J.; Fuhrhop, R. W.; Scherrer, D. E.; Wickline, S. A. *Acad. Radiol.* **2002**, *9*, S330.
(29) Winter, P. M.; Caruthers, S. D.; Yu, X.; Song, S. K.; Chen, J. J.; Miller, B.; Bulte, J. W. M.; Robertson, J. D.; Gaffney, P. J.; Wickline, S. A.; Lanza, G. M. *Magn. Reson. Med.* **2003**, *50*, 411.
(30) Jores, K.; Mehnert, W.; Drechsler, M.; Bunjes, H.; Johann, C.; Mader, K. *J. Controlled Release* **2004**, *95*, 217.
(31) Muller, R. H.; Mader, K.; Gohla, S. *Eur. J. Pharm. Biopharm.* **2000**, *50*, 161.
(32) zur Muhlen, A.; Schwarz, C.; Mehnert, W. *Eur. J. Pharm. Biopharm.* **1998**, *45*, 149.
(33) Akanni, M. S.; Okoh, E. K.; Burrows, H. D.; Ellis, H. A. *Thermochim. Acta* **1992**, *208*, 1.
(34) Binnemans, K.; Jongen, L.; Bromant, C.; Hinz, D.; Meyer, G. *Inorg. Chem.* **2000**, *39*, 5938.
(35) Mehrotra, K. N.; Sharma, N. *Pol. J. Chem.* **1996**, *70*, 1236.
(36) Mehrotra, K. N.; Shukla, R. K.; Chauhan, M. *Bull. Chem. Soc. Jpn.* **1995**, *68*, 1825.
(37) Nakamoto, K. *Infrared Spectra of Inorganic and Coordination Compounds*; Wiley: New York, 1963; p 198.
(38) Cotton, F. A. Wilkinson, G. *Advanced Inorganic Chemistry*, 5th ed.; Wiley: New York, 1988; p 483.
(39) Deacon, G. B.; Phillips, R. J. *Coord. Chem. Rev.* **1980**, *33*, 227.
(40) Saperstein, D. D. *J. Phys. Chem.* **1987**, *91*, 2922.
(41) Jongen, L.; Goderis, B.; Dolbnya, I.; Binnemans, K. *Chem. Mater.* **2003**, *15*, 212.
(42) Shannon, R. D. *Acta Crystallogr. A* **1976**, *A32*, 751.
(43) Upadhyaya, S. K.; Sharma, P. S. *J. Indian Chem. Soc.* **1993**, *70*, 735.
(44) Drummond, C. J.; Grieser, F.; Healy, T. W. *J. Chem. Soc. Faraday Trans. 1* **1989**, *85*, 521.
(45) Sinha, A. P. B. *Spectrosc. Inorg. Chem.* **1971**, *2*, 255.
(46) Cookson, D.; Kirby, N.; Knott, R.; Lee, M.; Schultz, D. *J. Synchrotron. Radiat.* **2006**, *13*, 440.
(47) Seddon, J. M.; Squires, A. M.; Conn, C. E.; Ces, O.; Heron, A. J.; Mulet, X.; Shearman, G. C.; Templer, R. H. *Philos. Trans. R. Soc. A* **2006**, *364*, 2635.
(48) *Modern NMR Techniques for Chemistry Research*; Derome, A. E., Ed.; Pergamon Press: Oxford, UK, 1987; Vol. 6, p 86.
(49) Koening, A. E. *J. Am. Chem. Soc.* **1914**, *36*, 951.
(50) Binnemans, K.; Gorller-Walrand, C. *Chem. Rev.* **2002**, *102*, 2303.
(51) Binnemans, K.; Gorllerwalrand, C. *Chem. Phys. Lett.* **1995**, *235*, 163.

JP906344U